arXiv:1110.2104v3 [astro-ph.SR] 9 Jan 2012

Impact of eV-mass sterile neutrinos on neutrino-driven supernova outflows

Irene Tamborra,[a] **Georg G. Raffelt,**[a] **Lorenz Hüdepohl**[b] **and Hans-Thomas Janka**[b]

[a]Max-Planck-Institut für Physik (Werner-Heisenberg-Institut)
Föhringer Ring 6, 80805 München, Germany
[b]Max-Planck-Institut für Astrophysik
Karl-Schwarzschild-Str. 1, 85748 Garching, Germany

E-mail: tamborra@mpp.mpg.de, raffelt@mpp.mpg.de,
lorenz@mpa-garching.mpg.de, thj@mpa-garching.mpg.de

Abstract. Motivated by recent hints for sterile neutrinos from the reactor anomaly, we study active-sterile conversions in a three-flavor scenario (2 active + 1 sterile families) for three different representative times during the neutrino-cooling evolution of the proto-neutron star born in an electron-capture supernova. In our "early model" (0.5 s post bounce), the ν_e-ν_s MSW effect driven by $\Delta m^2 = 2.35$ eV^2 is dominated by ordinary matter and leads to a complete ν_e-ν_s swap with little or no trace of collective flavor oscillations. In our "intermediate" (2.9 s p.b.) and "late models" (6.5 s p.b.), neutrinos themselves significantly modify the ν_e-ν_s matter effect, and, in particular in the late model, $\nu\nu$ refraction strongly reduces the matter effect, largely suppressing the overall ν_e-ν_s MSW conversion. This phenomenon has not been reported in previous studies of active-sterile supernova neutrino oscillations. We always include the feedback effect on the electron fraction Y_e due to neutrino oscillations. In all examples, Y_e is reduced and therefore the presence of sterile neutrinos can affect the conditions for heavy-element formation in the supernova ejecta, even if probably not enabling the r-process in the investigated outflows of an electron-capture supernova. The impact of neutrino-neutrino refraction is strong but complicated, leaving open the possibility that with a more complete treatment, or for other supernova models, active-sterile neutrino oscillations could generate conditions suitable for the r-process.

Contents

1   Introduction

Sterile neutrinos are hypothetical gauge-singlet fermions that could mix with one or more of the active states and thus show up in active-sterile flavor oscillations. Low-mass sterile neutrinos have been invoked to explain the excess $\bar{\nu}_e$ events in the LSND experiment [1–3] as well as the MiniBooNE excess events in both neutrino and antineutrino channels. Interpreted in terms of flavor oscillations, the MiniBooNE data require CP violation and thus no less than two sterile families [4–6]. However, these models show tension with other oscillation data and may require additional ingredients such as non-standard interactions [7]. Moreover, part of the parameter space has been excluded by IceCube data [8]. On the other hand, the cosmic microwave background anisotropies [9–13] and big-bang nucleosynthesis [14, 15] suggest cosmic excess radiation compatible with one family of sub-eV sterile neutrinos. However, for eV-mass sterile neutrinos to be cosmologically viable, additional ingredients are required [16].

     Our study is motivated by the most recent indication for the possible existence of eV-mass sterile neutrinos coming from a new analysis of reactor $\bar{\nu}_e$ spectra and their distance and energy variation [17–19]. The data suggest a ν_e-ν_s mixing of $\sin^2 2\theta \sim 0.14$ and a mass splitting of $\Delta m^2 \gtrsim 1.5$ eV^2. In the supernova (SN) context, these parameters imply that the ν_e flux would undergo MSW conversions to ν_s closer to the SN core than any other oscillation effects. (We assume that, because of cosmological neutrino mass limits, the sterile state is heavier than the active ones so that the MSW effect would occur between ν_e and ν_s and not between $\bar{\nu}_e$ and $\bar{\nu}_s$.) Even then, however, the conversion probably would not be close enough to the SN core to affect shock reheating during the accretion phase. Moreover, removing the ν_e flux would stabilize the remaining flux of active neutrinos against collective flavor conversions which anyway are likely irrelevant for shock reheating [20–23]. At a larger radius, the lost ν_e flux would be partly replenished by active-active MSW oscillations, in detail depending on the mixing parameters among active neutrinos. So while the ν_e flux arriving at Earth from the next nearby SN would be significantly modified, observational signatures would probably require a large ν_e detector, in contrast to the existing large detectors that

primarily measure the arriving $\bar{\nu}_e$ flux by inverse beta decay. Still, possible observational signatures may deserve a dedicated study.

We here focus on a different aspect of ν_e-ν_s oscillations that could have an interesting impact during the neutrino-cooling phase of the proto-neutron star (PNS). The neutrino-driven matter outflow contributes to SN nucleosynthesis and, in particular, it is a candidate site for the formation of elements beyond iron by the rapid neutron-capture process (for a review, see [24] and references therein). This "r-process" requires a neutron-rich environment, i.e. an electron fraction per baryon $Y_e < 0.5$, sufficiently large entropy to favor a high ratio of free neutrons to "seed" nuclei (the latter are usually iron-group nuclei reassembled from free nucleons and acting as starting points of neutron captures), and sufficiently fast timescales to lower the efficacy of converting alpha particles to heavier nuclei. In standard SN simulations, these conditions have remained elusive. The idea that removing the ν_e flux by active-sterile oscillations can favor a neutron-rich outflow environment is not new [25–31]. However, the used mass differences were larger and the possible impact of collective active-active oscillations [32] was not taken into account. On the other hand, several recent studies have considered the role of collective flavor oscillations (without sterile neutrinos) on nucleosynthesis processes like the r-process and the νp-process in SN outflows [33, 34].

In our study we explore the impact of ν_e-ν_s oscillations on the electron fraction Y_e, based on a self-consistent SN model and the corresponding flavor-dependent neutrino fluxes from a spherically symmetric (1D) simulation of an exploding electron-capture SN, which leaves behind a neutrino-cooling PNS [35]. To this end we begin in section 2 with a description of our electron capture SN reference model, we define our notation and fix the neutrino mixing parameters. In section 3 we describe the Y_e evolution in SN outflows. In section 4 we present our results for three representative times after core bounce ($t = 0.5$, 2.9 and 6.5 s). Conclusions and perspectives are presented in section 5.

2   Input for neutrino flavor evolution in electron-capture supernovae

Electron-capture supernovae, originating from low-mass progenitors (8–$10\,M_\odot$), might represent up to about 30% of all core-collapse supernovae [36, 37]. We use long-term simulations of a representative progenitor with mass $8.8\,M_\odot$ [35], performed with the equation of state of Shen et al. [38]. For the present study we chose Model Sf 21 (see reference [35] for further details; the number 21 denotes a recomputation of the published model with 21 energy bins in the neutrino transport instead of the standard 17 bins). In the chosen model, the accretion phase ends already at ~ 0.2 s post bounce when neutrino heating reverses the infall to an explosion, and the subsequent deleptonization and cooling of the PNS take ~ 10 s. In this section, we discuss our reference model for an electron-capture SN, the neutrino fluxes, and the flavor evolution equations.

2.1   Reference neutrino signal from electron-capture SNe

At a radius r, the unoscillated spectral number fluxes for flavor ν_β ($\beta = e, \bar{e}, x$ with $x = \mu$ or τ) are

$$F_{\nu_\beta}(E) = \frac{L_{\nu_\beta}}{4\pi r^2} \frac{f_{\nu_\beta}(E)}{\langle E_{\nu_\beta} \rangle} \ , \tag{2.1}$$

t	R_ν	L_{ν_e}	$L_{\bar{\nu}_e}$	L_{ν_x}	$\langle E_{\nu_e}\rangle$	$\langle E_{\bar{\nu}_e}\rangle$	$\langle E_{\nu_x}\rangle$	α_e	$\alpha_{\bar{e}}$	α_x
0.5	25	9.5	10.1	10.8	16.8	18.1	18.3	2.9	3.0	2.8
2.9	16	3.3	3.4	3.7	15.8	16.3	15.7	3.1	2.6	2.5
6.5	14.5	1	0.99	1.04	12.4	11.9	11.8	2.6	2.3	2.4

Table 1. Parameters for the three considered, representative post-bounce times (in seconds) of our SN explosion model. Neutrino-sphere radius R_ν in km (assumed equal for all flavors), flavor-dependent luminosities L_{ν_β} (in 10^{51} erg s^{-1}), average energies $\langle E_{\nu_\beta}\rangle$ (in MeV), and the spectral shape factor α_β are listed.

where L_{ν_β} is the luminosity for flavor ν_β, $\langle E_{\nu_\beta}\rangle$ the mean energy, and $f_{\nu_\beta}(E)$ a quasi-thermal spectrum. We describe it schematically in the form [39]

$$f_{\nu_\beta}(E) = \xi_\beta \left(\frac{E}{\langle E_{\nu_\beta}\rangle} \right)^{\alpha_\beta} e^{-(\alpha_\beta+1)E/\langle E_{\nu_\beta}\rangle} \ . \tag{2.2}$$

The parameter α_β is defined by $\langle E_{\nu_\beta}^2\rangle/\langle E_{\nu_\beta}\rangle^2 = (2+\alpha_\beta)/(1+\alpha_\beta)$ and ξ_β is a normalization factor such that $\int dE\, f_{\nu_\beta}(E) = 1$. We choose three representative times during the PNS cooling: $t = 0.5$, 2.9 and 6.5 s after core bounce. In table 1, the neutrino-sphere radius, the luminosity L_{ν_β}, the average energies $\langle E_{\nu_\beta}\rangle$, and the factor α_β are reported. Concerning the neutrino emission geometry, we adopt the spherically-symmetric bulb model [40], with the neutrino-sphere radii assumed equal for all active flavors.

2.2 Neutrino mixing parameters and flavor evolution equations

Our work is motivated by the reactor anti-neutrino anomaly that requires, if interpreted in terms of sterile neutrinos ν_s, sizable ν_e–ν_s mixing. For simplicity we will ignore possible mixings of ν_s with other active flavors. The mass difference would have to be in the eV range, so cosmological hot dark matter limits imply that the sterile state would have to be heavier than the active flavors. Besides ν_e–ν_s oscillations, we also include active-active oscillations driven by the atmospheric mass difference between ν_e and ν_x and the mixing angle Θ_{13}. The ν_μ and ν_τ fluxes in a SN are very similar and these two flavors play symmetric roles. Therefore, it is useful to define a linear combination that is essentially identical with the m_3 mass eigenstate and mixes with ν_e by means of the small Θ_{13} mixing angle, and another combination that mixes through the solar angle Θ_{12} and is separated with the solar mass difference $\delta m_{\rm sol}$. Oscillations driven by these parameters tend to take place at a larger radius and likely do not affect SN nucleosynthesis. Overall, therefore, we study a 3-flavor problem consisting of ν_e, ν_x and ν_s with the mass splittings

$$\delta m_{\rm atm}^2 = -2 \times 10^{-3} \ {\rm eV}^2 \ , \tag{2.3}$$

$$\delta m_{\rm s}^2 = 2.35 \ {\rm eV}^2 \ , \tag{2.4}$$

where the latter is representative for the reactor-inspired values [17]. Note that we assume normal hierarchy for the sterile mass-squared difference $\delta m_{\rm s}^2 > 0$ and inverted hierarchy for the atmospheric difference, $\delta m_{\rm atm}^2 < 0$ for the atmospheric sector. The associated "high" (H)

and "sterile" (S) vacuum oscillation frequencies are then

$$\omega_{\mathrm{H}} = \frac{\delta m_{\mathrm{atm}}^2}{2E} = -\frac{5.07}{E(\mathrm{MeV})}\mathrm{km}^{-1} \; , \tag{2.5}$$

$$\omega_{\mathrm{S}} = \frac{\delta m_{\mathrm{s}}^2}{2E} = \frac{5.96 \times 10^3}{E(\mathrm{MeV})}\mathrm{km}^{-1} \; , \tag{2.6}$$

whereas the usual "low" (L) frequency corresponds to the solar mass difference. For the active-sterile mixing we use

$$\sin^2 2\Theta_{14} = 0.165 \; . \tag{2.7}$$

We assume a small mixing between the active flavors,

$$\sin^2 \Theta_{13} = 10^{-4} \; . \tag{2.8}$$

In this case the MSW effect driven by this mixing angle is non-adiabatic, i.e. we only focus on active-sterile MSW oscillations and collective active-active oscillations. Recent hints for a not-very-small value for Θ_{13} [41] would imply that we also need to include flavor conversion by the active-active MSW effect, but this has little impact on our results.

We treat neutrino oscillations in terms of the usual matrices of neutrino densities ρ_E for each neutrino mode with energy E where diagonal elements are neutrino densities, off-diagonal elements encode phase information caused by flavor oscillations. Moreover, we work in the single-angle approximation where it is assumed that all neutrinos feel the same average neutrino-neutrino refractive effect. The radial flavor variation of the quasi-stationary neutrino flux is given by the "Schrödinger equation"

$$i\partial_r \rho_E = [\mathsf{H}_E, \rho_E] \quad \text{and} \quad i\partial_r \bar{\rho}_E = [\bar{\mathsf{H}}_E, \bar{\rho}_E] \, , \tag{2.9}$$

where an overbar refers to antineutrinos and sans-serif letters denote 3×3 matrices in flavor space consisting of ν_e, ν_x and ν_s. The initial conditions are $\rho_E = \mathrm{diag}(n_{\nu_e}, n_{\nu_x}, 0)$ and $\bar{\rho}_E = \mathrm{diag}(n_{\bar{\nu}_e}, n_{\bar{\nu}_x}, 0)$. The Hamiltonian matrix contains vacuum, matter, and neutrino–neutrino terms

$$\mathsf{H}_E = \mathsf{H}_E^{\mathrm{vac}} + \mathsf{H}_E^{\mathrm{m}} + \mathsf{H}_E^{\nu\nu} \; . \tag{2.10}$$

In the flavor basis, the vacuum term is a function of the mixing angles and the mass-squared differences

$$\mathsf{H}_E^{\mathrm{vac}} = \mathsf{U} \, \mathrm{diag}\left(-\frac{\omega_{\mathrm{H}}}{2}, +\frac{\omega_{\mathrm{H}}}{2}, \omega_{\mathrm{S}}\right) \mathsf{U}^\dagger \; , \tag{2.11}$$

where U is the unitary mixing matrix transforming between the mass and the interaction basis. The matter term includes both charged-current (CC) and neutral-current (NC) contributions and it is in the flavor basis spanned by (ν_e, ν_x, ν_s)

$$\mathsf{H}^{\mathrm{m}} = \sqrt{2}G_{\mathrm{F}} \, \mathrm{diag}(N_e - \frac{N_n}{2}, -\frac{N_n}{2}, 0) \; , \tag{2.12}$$

where N_e is the net electron number density (electrons minus positrons), and N_n the neutron density.

In all neutral media, $Y_e = Y_p$ and $Y_n = 1 - Y_e$, where Y_j is the number density of particle species j relative to baryons. The local electron fraction is

$$Y_e(r) = \frac{N_e(r)}{N_e(r) + N_n(r)} \; . \tag{2.13}$$

Inserting the previous expression for Y_e in equation (2.12), the matter Hamiltonian becomes

$$\mathsf{H}^{\mathrm{m}} = \sqrt{2}G_{\mathrm{F}}N_b \, \mathrm{diag}\left(\frac{3}{2}Y_e - \frac{1}{2}, \frac{1}{2}Y_e - \frac{1}{2}, 0\right) \, , \qquad (2.14)$$

where N_b is the baryon density. The matter potential can be positive or negative. For $Y_e > 1/3$ it is ν_e that can undergo an active-sterile Mikheev-Smirnov-Wolfenstein (MSW) resonance, whereas for $Y_e < 1/3$ it is $\bar{\nu}_e$ [42].

The corresponding 3×3 matrix caused by neutrino-neutrino interactions vanishes for all elements involving sterile neutrinos [43], i.e. $\mathsf{H}_{es}^{\nu\nu} = \mathsf{H}_{xs}^{\nu\nu} = \mathsf{H}_{ss}^{\nu\nu} = 0$, and only the 2×2 block involving the active flavors is non-zero. In particular, the only non-vanishing off-diagonal element of the 3×3 matrix is $\mathsf{H}_{ex}^{\nu\nu}$.

In summary, the matter plus neutrino-neutrino part of the Hamiltonian has the diagonal elements

$$\mathsf{H}_{ee}^{\mathrm{m}+\nu\nu} = \sqrt{2}G_{\mathrm{F}}\left[N_b\left(\frac{3}{2}Y_e - \frac{1}{2}\right) + 2(N_{\nu_e} - N_{\bar{\nu}_e}) + (N_{\nu_x} - N_{\bar{\nu}_x})\right] \, , \qquad (2.15)$$

$$\mathsf{H}_{xx}^{\mathrm{m}+\nu\nu} = \sqrt{2}G_{\mathrm{F}}\left[N_b\left(\frac{1}{2}Y_e - \frac{1}{2}\right) + (N_{\nu_e} - N_{\bar{\nu}_e}) + 2(N_{\nu_x} - N_{\bar{\nu}_x})\right] \, , \qquad (2.16)$$

whereas initially the off-diagonal elements vanish. These expressions represent the energy shift of ν_e or ν_x relative to ν_s caused by matter and neutrino refraction.

3 Electron fraction evolution

The material in a fluid element moving away from the SN core will experience three stages of nuclear evolution. Near the surface of the neutron star, typically the material is very hot and essentially all of the baryons are in the form of free nucleons. As the material flows away from the neutron star, it cools. When the temperature $T < 1$ MeV, α particles begin to assemble. As the fluid flows farther out and cools further, heavier nuclei begin to form. Around half of the nuclei with masses $A > 100$ are supposed to be created by the r-process, requiring neutron-rich conditions. In this section, we introduce the Y_e evolution equation to study whether the impact of sterile neutrinos can help to produce such an environment.

Having in mind the overall evolution of abundances with radius and time, namely that close to the neutrino sphere only free nucleons exist, then alpha-particles begin to form and afterwards (some) heavy nuclei, the electron abundance introduced in equation (2.13) can be expressed as

$$Y_e = X_p + \frac{X_\alpha}{2} + \sum_h \frac{Z_h}{A_h} X_h \, . \qquad (3.1)$$

Here X_p (X_α) is the mass fraction of free protons (alpha particles) and Z_h and A_h are the charge and mass number of nuclear species h. The summation runs over all nuclear species h heavier than α particles. However, at the conditions common to neutrino-heated outflows (in particular in the region where neutrino interactions have the biggest impact on Y_e), free nucleons and alpha particles typically account for most of the baryons.

The CC weak interactions alter the electron fraction by converting neutrons to protons and vice versa. The electron abundance Y_e in neutrino-heated material flowing away from the neutron star is set by a competition between the rates of the following neutrino and

antineutrino capture reactions on free nucleons, assuming that the reactions of neutrinos on nuclei are negligible,

$$\nu_e + n \to p + e^- \ , \tag{3.2}$$

$$\bar{\nu}_e + p \to n + e^+ \ , \tag{3.3}$$

and by the associated reverse processes. Because of slow time variations of the outflow conditions during the PNS cooling phase, a near steady-state situation applies and the Y_e rate-of-change within an outflowing mass element may be written as [44]

$$\frac{dY_e}{dt} = v(r)\frac{dY_e}{dr} \simeq (\lambda_{\nu_e} + \lambda_{e^+})Y_n^{\mathrm{f}} - (\lambda_{\bar{\nu}_e} + \lambda_{e^-})Y_p^{\mathrm{f}} \ , \tag{3.4}$$

where $v(r)$ is the velocity of the outflowing mass element and Y_n^{f} and Y_p^{f} are the abundances of free nucleons. The forward rates of the neutrino capture processes of equations (3.2) and (3.3) are [44]

$$\lambda_{\nu_e} \simeq \frac{L_{\nu_e}}{4\pi r^2 \langle E_{\nu_e} \rangle} \langle \sigma_{\nu_e n}(r) \rangle \ , \tag{3.5}$$

$$\lambda_{\bar{\nu}_e} \simeq \frac{L_{\bar{\nu}_e}}{4\pi r^2 \langle E_{\bar{\nu}_e} \rangle} \langle \sigma_{\bar{\nu}_e p}(r) \rangle \ . \tag{3.6}$$

The rates for the reverse processes (electron and positron capture rates on free nucleons) are approximately [44]

$$\lambda_{e^-} \simeq 1.578 \times 10^{-2} \ \mathrm{s}^{-1} \left(\frac{T_e}{m_e}\right)^5 e^{(-1.293+\mu_e)/T_e} \left(1 + \frac{0.646 \ \mathrm{MeV}}{T_e} + \frac{0.128 \ \mathrm{MeV}^2}{T_e^2}\right) \ , \tag{3.7}$$

$$\lambda_{e^+} \simeq 1.578 \times 10^{-2} \ \mathrm{s}^{-1} \left(\frac{T_e}{m_e}\right)^5 e^{(-0.511-\mu_e)/T_e}$$
$$\times \left(1 + \frac{1.16 \ \mathrm{MeV}}{T_e} + \frac{0.601 \ \mathrm{MeV}^2}{T_e^2} + \frac{0.178 \ \mathrm{MeV}^3}{T_e^3} + \frac{0.035 \ \mathrm{MeV}^4}{T_e^4}\right) \ , \tag{3.8}$$

where μ_e is the relativistic electron chemical potential (in MeV).

The electron temperature profile is extracted from the hydrodynamical simulation for Model Sf 21 of [35] and is shown in figure 1 for the considered outflow trajectories at different times after core bounce. The electron chemical potential has been computed by inverting the equation [45]

$$Y_e = \frac{8\pi}{3N_b} T_e^3 \eta(\eta^2 + \pi^2) \ , \tag{3.9}$$

where $\eta = \mu_e/T$ is the electron degeneracy parameter.

Though the details are more complex, Y_e at small radii is mainly determined by the e^- and e^+ capture rates whereas at larger radii the reverse neutrino-capture reactions dominate. Note that in equation (3.4) the nucleons involved in the β-reactions are free. Including the corrections due to nucleons bound in α particles, the free proton and neutron abundances are

$$Y_p^{\mathrm{f}} = Y_e - \frac{X_\alpha}{2} \quad \text{and} \quad Y_n^{\mathrm{f}} = 1 - Y_e - \frac{X_\alpha}{2} \ , \tag{3.10}$$

where X_α is the mass fraction of α particles. Assuming that nickel-56 is the most abundant among the heavy nuclei, we have tested that the correction to Y_e due to nuclei heavier than α
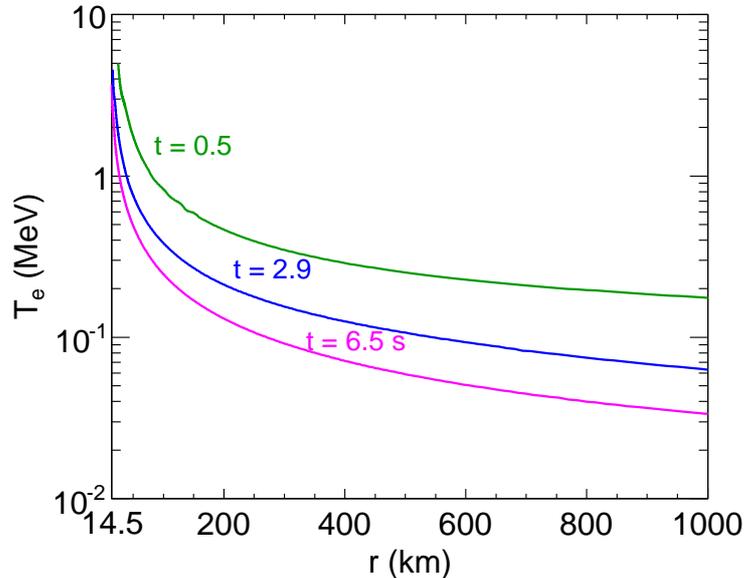
Figure 1. Electron temperature as function of radius from the hydrodynamical simulation of Model Sf 21 [35] for $t = 0.5$, 2.9 and 6.5 s after bounce.

t	R_ν	Y_e $(\times 10^{-2})$
0.5	25	5.47
2.9	16	3.23
6.5	14.5	2.33

Table 2. Initial electron abundance at the neutrino sphere R_ν (in km) for our three considered post-bounce times (in s).

particles is negligible. As the electron temperature, the mass fractions of α particles (and of heavy nuclei for the test) are taken from the hydrodynamical simulation of Model Sf 21 of [35]. Because the dominant abundances are free neutrons and protons and the differences of the Y_e evolution with and without neutrino oscillations are relatively small, this is a reasonable approximation, and a consistent treatment of the composition evolution would yield only minor corrections.

4   Results

In order to study the impact of sterile neutrinos on Y_e and on the neutrino fluxes, we discretize the coupled evolution equations (2.9) in the energy range 1–60 MeV and solve them by numerical integration together with equation (3.4). The initial conditions for Y_e from the hydrodynamical simulation are reported in table 2. The un-oscillated neutrino fluxes are fixed by the SN model described in section 2 according to the data given in table 1 for $t = 0.5$, 2.9 and 6.5 s. We consider two possible scenarios: one "with neutrino oscillations"
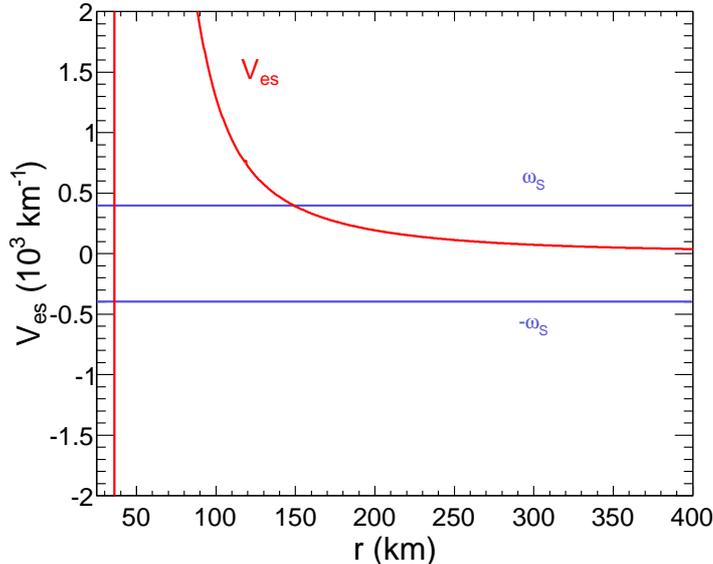
Figure 2. Refractive energy difference V_{es} between ν_e and ν_s for the snapshot $t = 0.5$ s. The horizontal line marks $\pm\omega_S$ for a typical neutrino energy of 15 MeV.

where we include the dynamical feedback on Y_e due to neutrino oscillations and the other one "without neutrino oscillations."

4.1 Early cooling phase ($t = 0.5$ s)

Figure 2 shows the radial profile of the refractive energy difference $V_{es} = H_{ee}^{\mathrm{m}+\nu\nu} - H_{ss}^{\mathrm{m}+\nu\nu} = H_{ee}^{\mathrm{m}+\nu\nu}$ between ν_e and ν_s as given in equation (2.15). This result already includes a self-consistent solution for Y_e caused by neutrino oscillations. The horizontal line marks ω_S for a representative neutrino energy of 15 MeV. An MSW resonance arises for both neutrinos and antineutrinos close to the neutrino-sphere. However, here the effective potential varies extremely fast because of the sudden rise of Y_e, preventing any significant flavor conversion (extremely non-adiabatic condition). At larger radii, a second resonance occurs for $r < 300$ km, but only for neutrinos, causing adiabatic flavor conversion. Therefore, we expect a larger flavor modification in the neutrino sector than in the antineutrino one.

Figure 3 shows the radial profile of the ν_e–ν_x refractive energy difference caused by matter alone

$$V_{ex}^{\mathrm{m}} = \sqrt{2}\, G_{\mathrm{F}}\, Y_e N_b\,, \tag{4.1}$$

including the self-consistent solution for Y_e. In the active-active sector, collective neutrino oscillations will occur. Their relevance is not correctly measured by the refractive energy difference $V_{ex}^{\nu\nu} = \sqrt{2}\, G_{\mathrm{F}}\, (N_{\nu_e} - N_{\bar{\nu}_e} - N_{\nu_x} + N_{\bar{\nu}_x})$ because collective effects are important even if this quantity vanishes due to the off-diagonal refractive index. One way to express the possible relevance of collective oscillations is in terms of the quantity

$$\mu = \sqrt{2}\, G_{\mathrm{F}}\, (N_{\nu_e} + N_{\bar{\nu}_e} + N_{\nu_x} + N_{\bar{\nu}_x})\,, \tag{4.2}$$
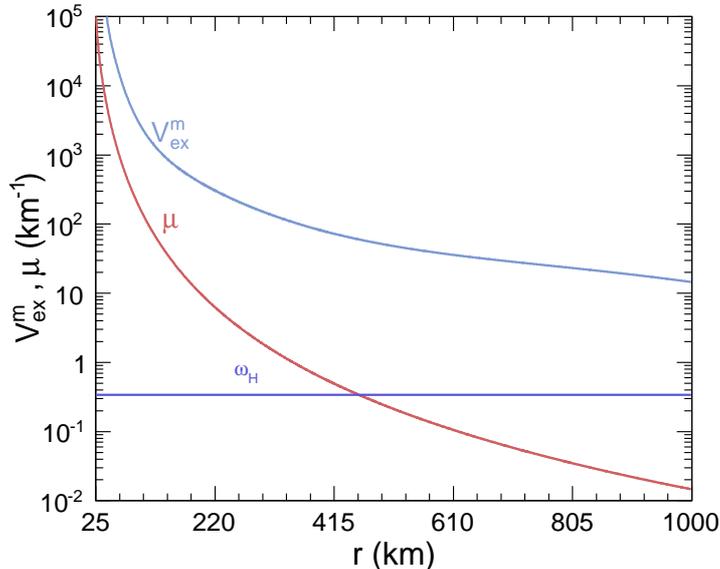
Figure 3. Refractive ν_e–ν_x energy difference caused by matter, V_{ex}^{m}, and the estimate μ for the neutrino-neutrino interaction energy for the $t = 0.5$ s model. The horizontal line marks ω_{H} for a typical neutrino energy of 15 MeV.

although somewhat different definitions of μ have been used in the literature. The potential μ is plotted in figure 3 as a function of the radius in order to give a comparison of the active neutrino abundance with respect to the electron one. For sake of simplicity, N_{ν_β} are fixed to their initial values since the correction due to neutrino density variations does not change the ratio between μ and V_{ex}^{m}. The horizontal line marks ω_{H} for the neutrino energy 15 MeV. No MSW resonance in the atmospheric sector is expected and the matter potential is always larger than μ.

In figure 4 we show the spectra for neutrinos (left) and antineutrino (right). The top panels show the primary spectra at the neutrino-sphere (no oscillations). Below we show the oscillated spectra when matter refraction is included, causing an almost complete MSW swap between ν_e and ν_s, but hardly any conversion between $\bar\nu_e$ and $\bar\nu_s$. Finally in the bottom panel we show the result after including neutrino-neutrino interactions in the single-angle approximation, causing no further modification. After the ν_e–ν_s MSW conversion, the e–x difference spectrum is very asymmetric between neutrinos and antineutrinos, essentially suppressing collective conversions. Moreover, $F_{\nu_e}(E) < F_{\nu_x}(E)$ and the same is true for $\bar\nu$. The evolution is therefore inhibited because the system is close to a stable equilibrium point [46, 47]. Given the initial conditions produced by the active-sterile MSW effect for the subsequent collective oscillations, we expect that any multi-angle treatment might produce only a smearing of the spectral features without changing the hierarchy among the fluxes of different flavors [48, 49]. In fact the large asymmetry between ν_e and ν_x fluxes (and the same for $\bar\nu$) is responsible for inhibiting any possible flavor decoherence effect [50].

Figure 5 shows the effect of oscillations on the Y_e profile. The MSW swap between ν_e and ν_s almost completely removes the original ν_e flux and pushes the matter outflow to
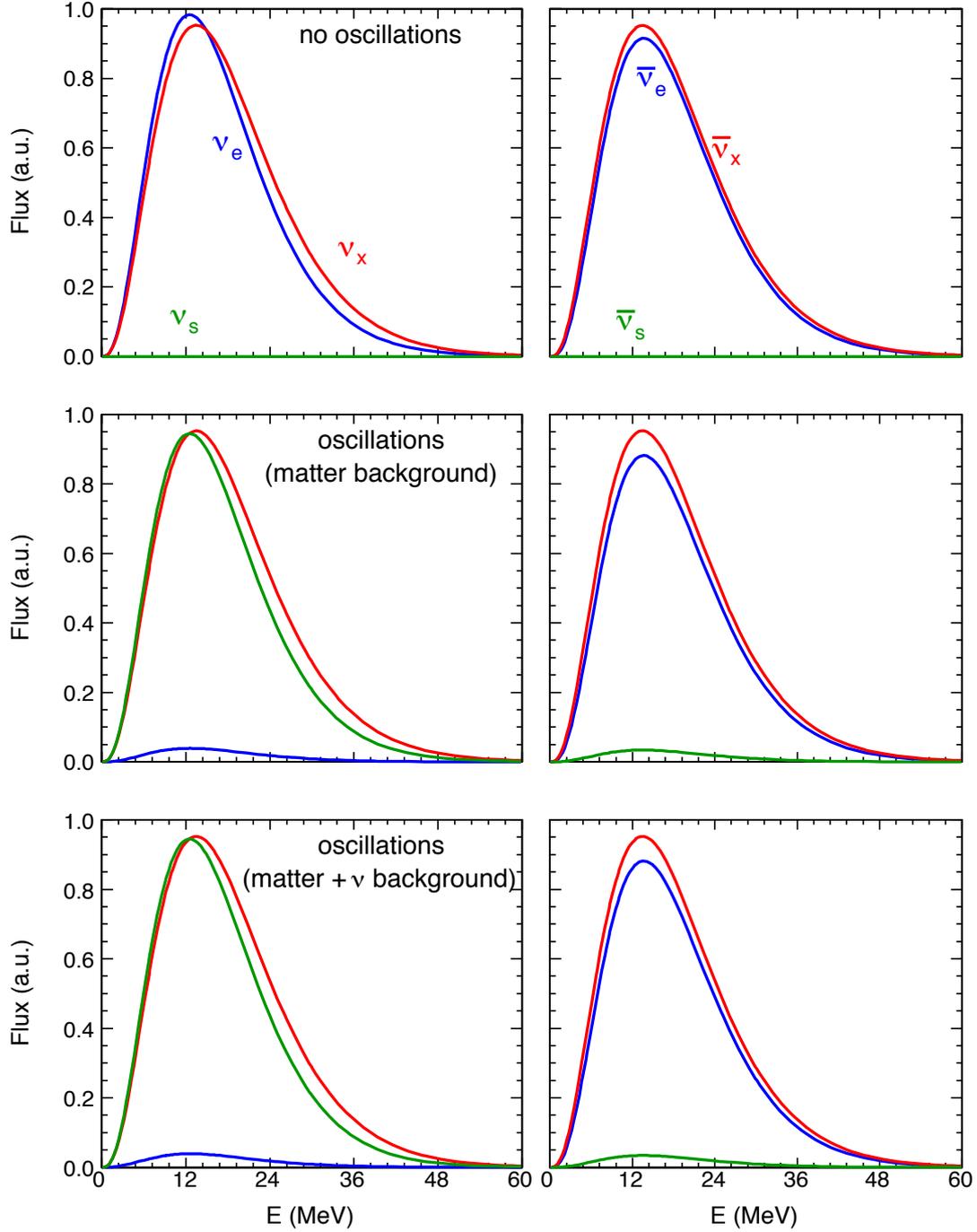
Figure 4. Spectra for neutrinos (left) and antineutrinos (right) at $r = 1000$ km in arbitrary units (a.u.) for the 0.5 s model. Top: No oscillations. Middle: Oscillated spectra, including only the matter effect. Bottom: ν–ν interactions are also included, but cause no visible difference.

a more neutron-rich environment, although not far enough to establish obviously favorable
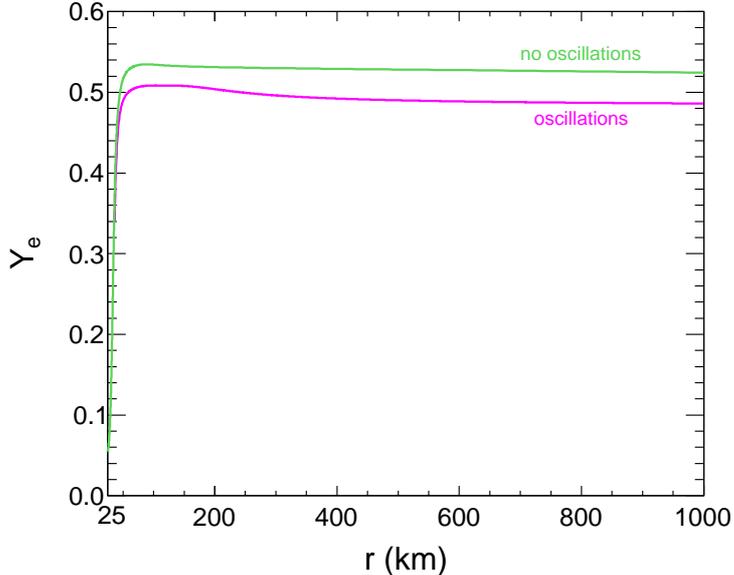
Figure 5. Electron abundance for the $t = 0.5$ s model, with and without oscillations.

conditions for an r-process.

4.2 Intermediate cooling phase ($t = 2.9$ s)

We next turn to a snapshot during the intermediate cooling phase at $t = 2.9$ s post bounce. In figures 6–10 we show the analogous information as previously for the early cooling phase. There are several new effects. One is that the refractive difference between ν_e and ν_s quickly drops in an almost step-like feature, caused by ν_e–ν_s MSW conversions (figure 6). Another is that the ν_e–ν_x refractive energy difference caused by matter is now much smaller, allowing for an MSW effect between the two active flavors in the neutrino sector for the chosen hierarchy (figure 7). The neutrino background is responsible for increasing the $\bar{\nu}_e$ flux with respect to the case with only matter and for averaging out the $\bar{\nu}_x$ and $\bar{\nu}_e$ fluxes.

In figure 10 the electron abundance is plotted as a function of the radius. The Y_e profile is lowered compared to the no-oscillation case. In particular, when $\nu\nu$ refraction is included, the asymptotic Y_e value, due to the increase of $\bar{\nu}_e$ flux, is more significantly shifted below 0.5 than at the earlier time of 0.5 s after bounce.

For comparison, in figure 9 the neutrino and antineutrino fluxes are shown for larger $\sin^2 \Theta_{13}$. In this case the MSW ν_e–ν_x conversion is adiabatic and as a result, the matter-only oscillations not only lead to an almost complete swap of ν_s to ν_e, but in addition a partial ν_e–ν_x swap. Including neutrino-neutrino refraction, since collective effects and MSW resonances are occurring all in the same spatial range, a spectral swap with two splits emerges, one in the neutrino sector at about 26 MeV, the other in the anti-neutrino sector at about 6 MeV. However, the increase of the ν_e flux at high energies counter-balances the increase of the $\bar{\nu}_e$ flux in such a way that the resultant Y_e does slightly change but without modifying our conclusions.
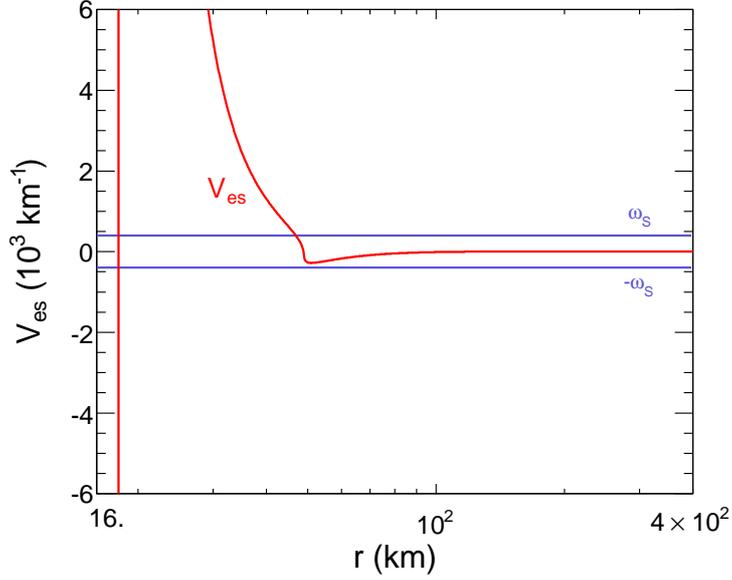
Figure 6. Refractive energy difference V_{es} between ν_e and ν_s for the snapshot $t = 2.9$ s. The horizontal line marks $\pm\omega_S$ for a typical neutrino energy of 15 MeV.
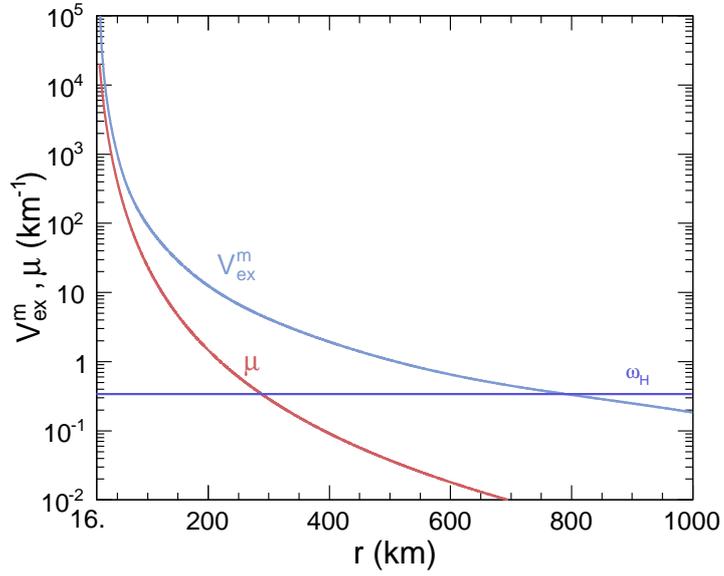

Figure 7. Refractive ν_e–ν_x energy difference caused by matter, V_{ex}^{m}, and the estimate μ for the neutrino-neutrino interaction energy for the $t = 2.9$ s model. The horizontal line marks ω_{H} for a typical neutrino energy of 15 MeV.
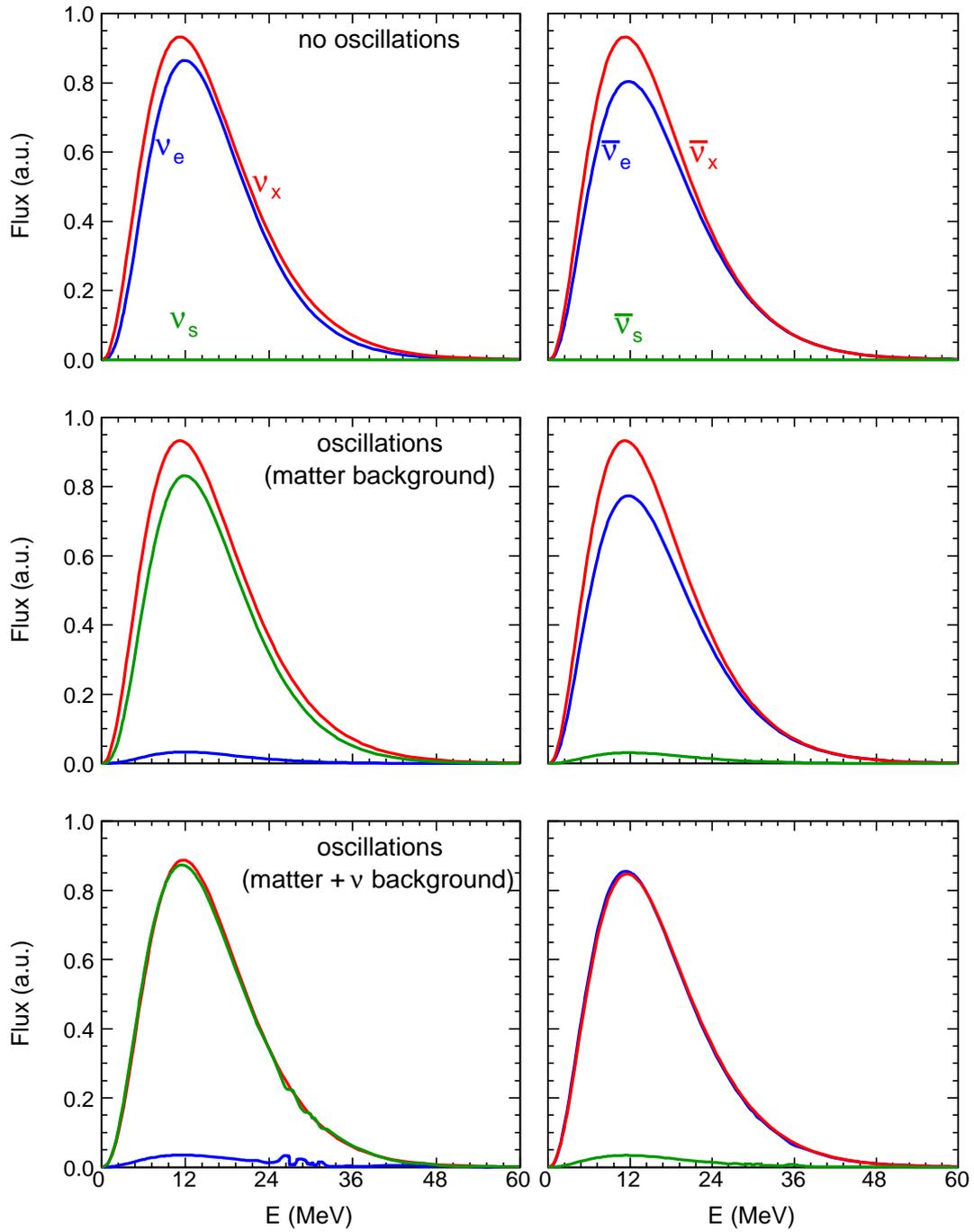
Figure 8. Energy spectra for $t = 2.9$ s as in figure 4.
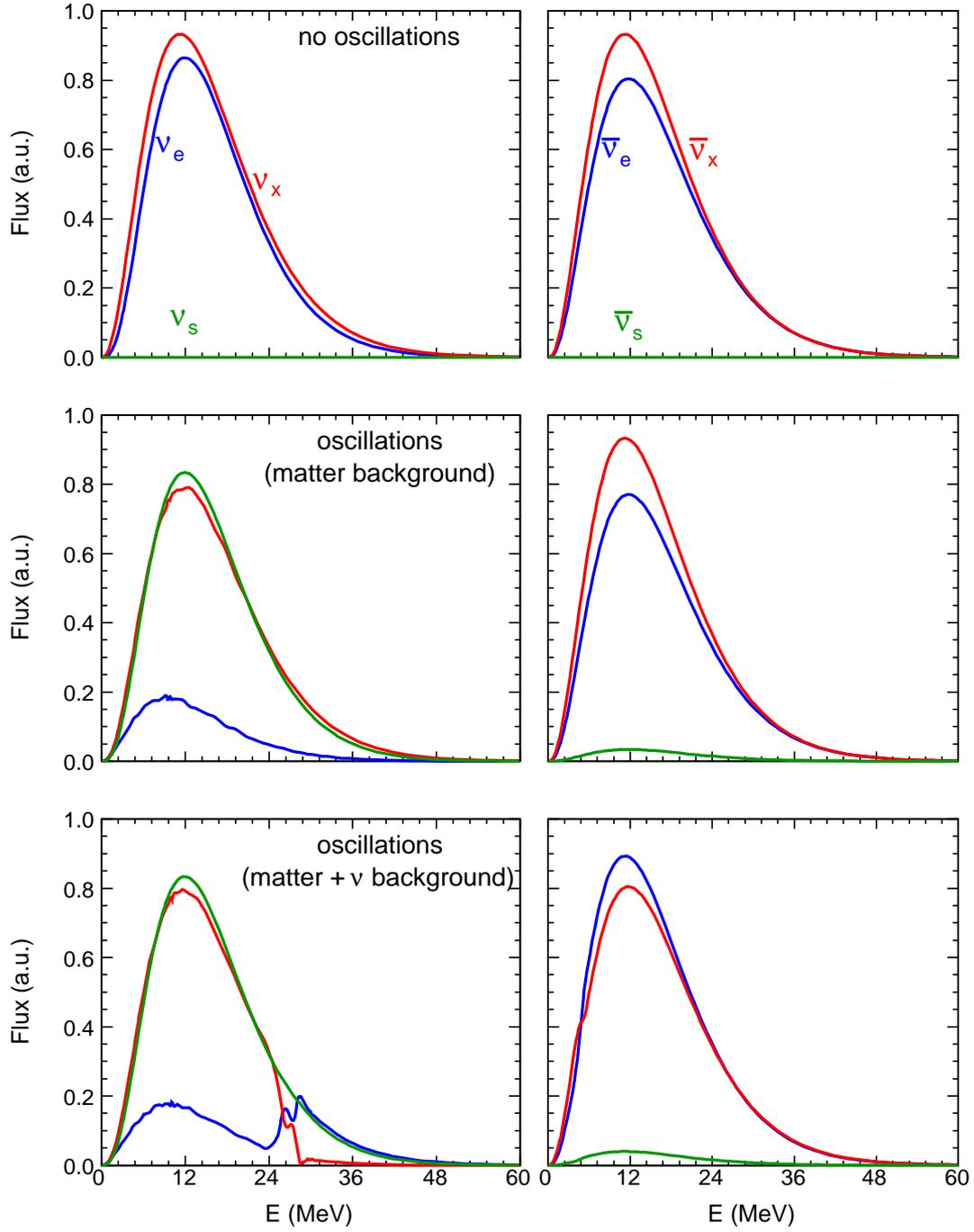
Figure 9. Same as figure 8 with $\sin^2 \Theta_{13} = 10^{-2}$ instead of our usual value $\sin^2 \Theta_{13} = 10^{-4}$.
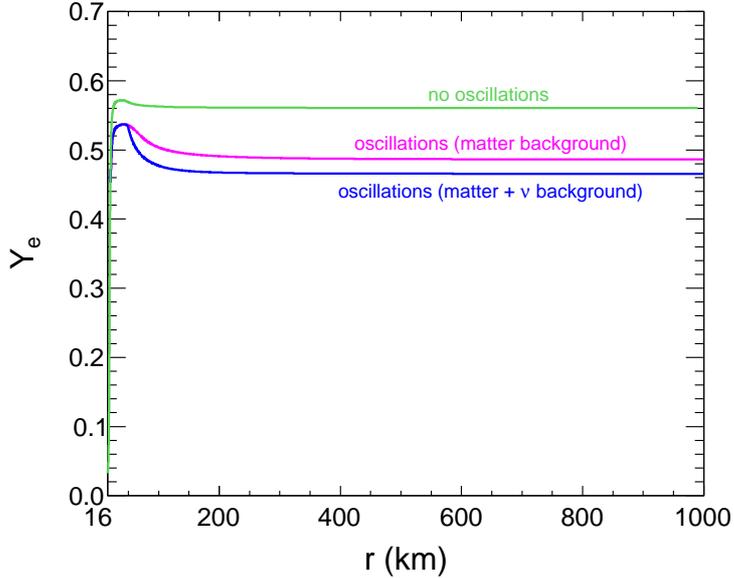
Figure 10. Electron abundance for the $t = 2.9$ s model for different oscillation cases as indicated.

4.3 Late cooling phase ($t = 6.5$ s)

Finally, we consider the late cooling phase for a snapshot at $t = 6.5$ s post bounce. In figures 11–14 we show the analogous information as in the previous cases. The active-sterile MSW effect once more leads to an almost complete ν_e–ν_s swap, if we include only the ordinary matter effect. However, once we include $\nu\nu$ refraction, the results change quite dramatically. The active-sterile energy difference again drops quickly at a critical radius because neutrinos contribute significantly to the matter effects and the MSW conversion shifts the total matter effect to zero and then has oscillatory features, apparently causing parametric resonance effects in subsequent neutrino oscillations. Flavor conversions differ for each energy mode, inducing wiggles in the energy spectra shown on the bottom panels of figure 13. As a result, the oscillated spectra are mixed up and, in particular, the ν_e and ν_x spectra are almost coincident. It is $\nu\nu$ interactions that are responsible for repopulating the ν_e spectrum and, consequently increase the Y_e value with respect to the case with only matter background as visible in figure 14. The asymptotic Y_e value drops far below 0.5 when only the matter effect is considered, but including $\nu\nu$ interactions it is pushed back up above 0.5, although in both cases Y_e is lowered relative to the no-oscillation case.
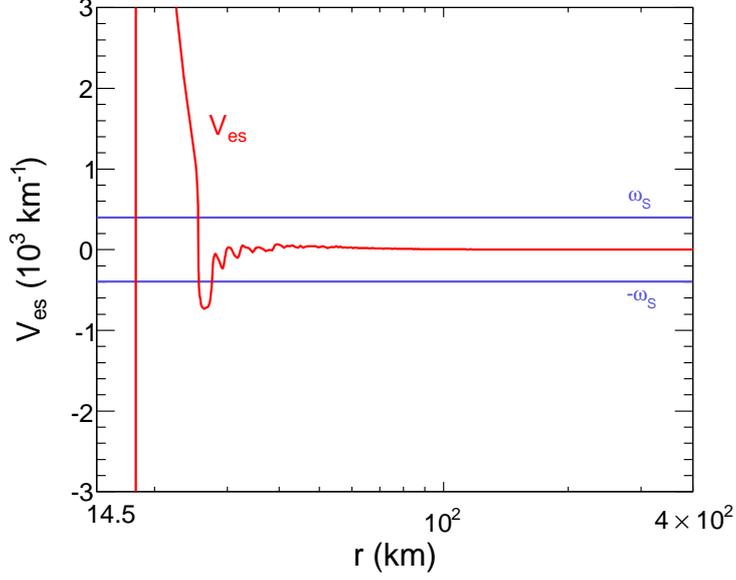
Figure 11. Refractive energy difference V_{es} between ν_e and ν_s for the snapshot $t = 6.5$ s. The horizontal line marks $\pm\omega_S$ for a typical neutrino energy of 15 MeV.
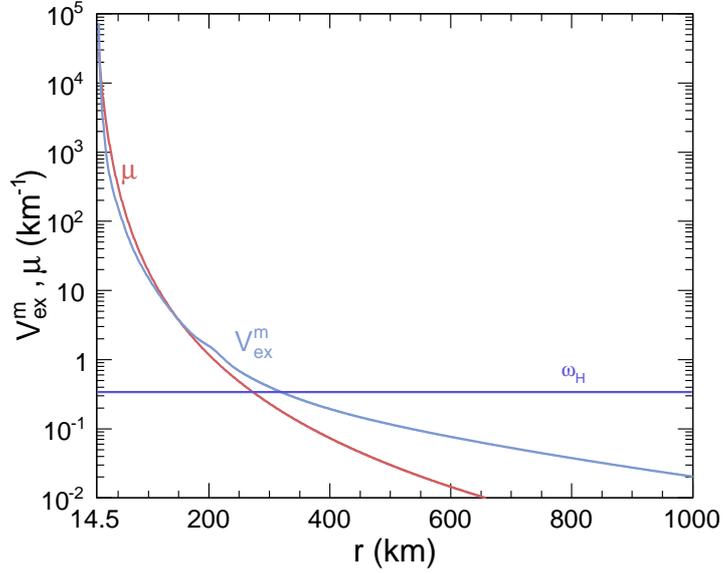

Figure 12. Refractive ν_e–ν_x energy difference caused by matter, V_{ex}^m, and the estimate μ for the neutrino-neutrino interaction energy for the $t = 6.5$ s model. The horizontal line marks ω_H for a typical neutrino energy of 15 MeV.
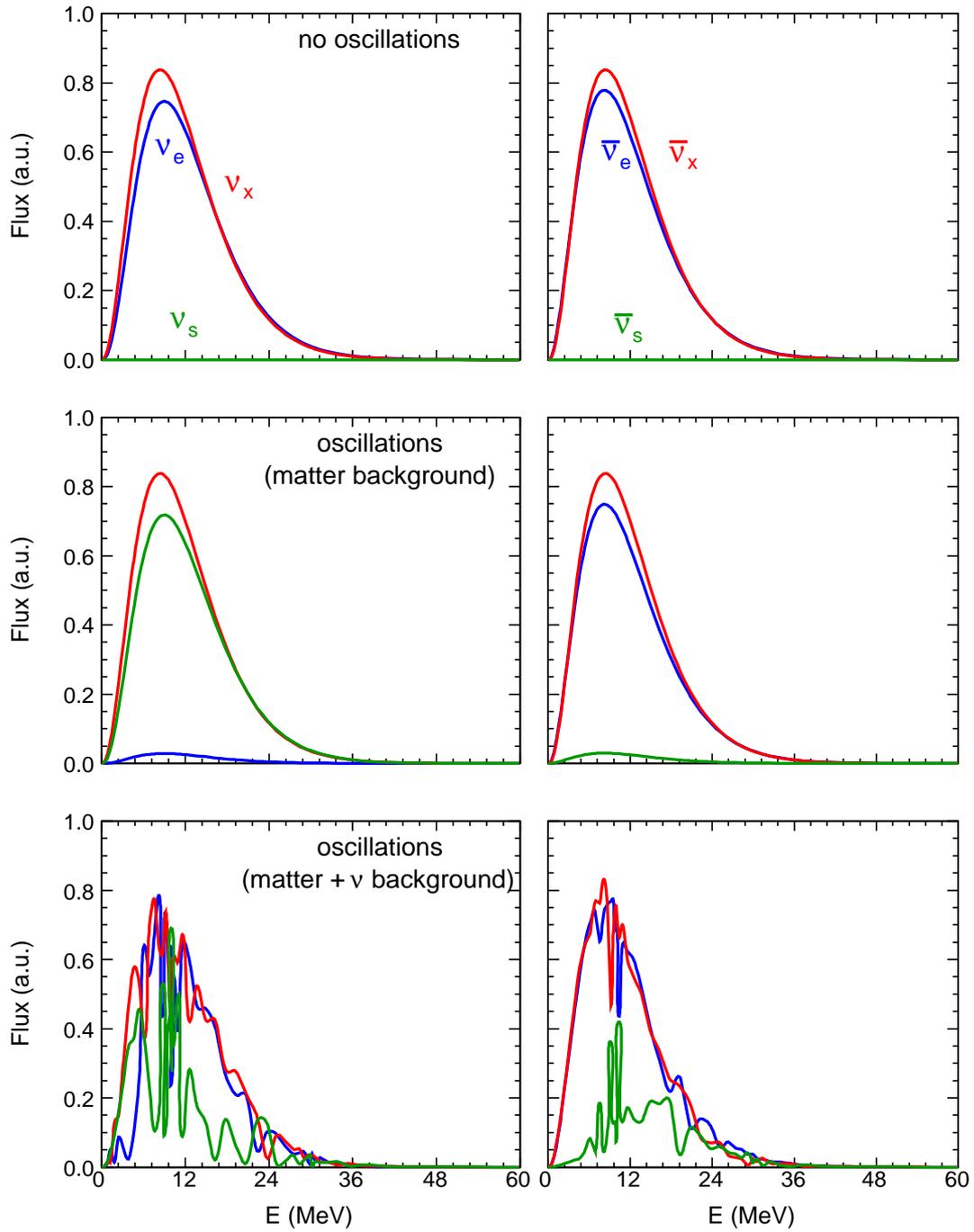
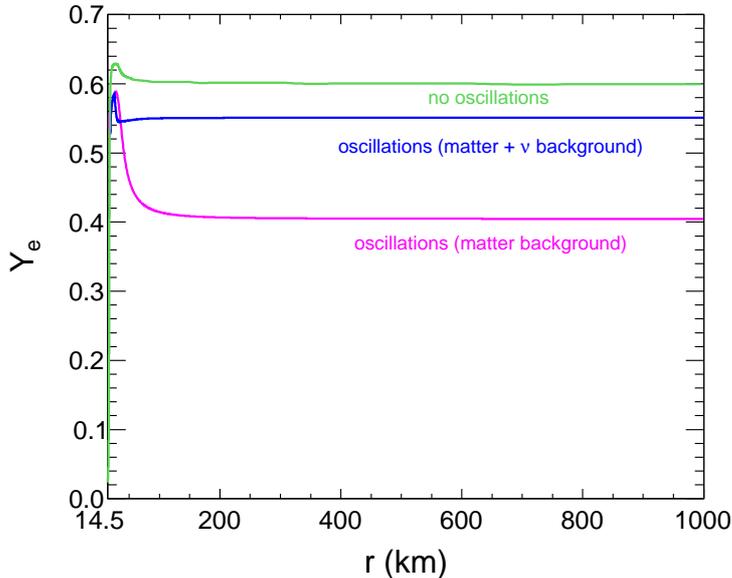**Figure 13**. Energy spectra for $t = 6.5$ s as in figure 4.

Figure 14. Electron abundance evolution for the $t = 6.5$ s model for different oscillation cases as indicated.

5 Conclusions

Motivated by recent hints for the existence of sterile neutrinos, and in particular the antineutrino reactor anomaly, we have studied flavor oscillations within a three-flavor (ν_e, ν_x, ν_s) scheme in the context of an electron-capture SN model, focussing on the neutrino-cooling phase of the nascent neutron star. We have included ν_e-ν_s mixing with parameters suggested by the reactor anomaly and active-active mixing representing 1–3 oscillations driven by the atmospheric mass difference and a small Θ_{13} angle. Our main goal was the determination of neutrino flux and spectral changes and their impact on the evolution and asymptotic value of Y_e in the neutrino-driven wind ejecta. Their modification is relevant for nucleosynthesis in SN outflows. We have studied three snapshots that are representative for the early, intermediate, and late cooling stages.

Even in our simplified neutrino mixing scheme, the results depend sensitively and in complicated ways on the detailed matter profile and neutrino fluxes and spectra. In the early phase after the onset of the explosion, oscillations are driven almost entirely by the ordinary matter effect and lead to a simple ν_e–ν_s MSW conversion. In the latter cases, neutrinos contribute significantly to the refractive energy shifts. One result is that the overall ν_e–ν_s energy difference drops to zero when some of the MSW conversion is complete and in this way oscillations feed back on themselves. The switch-off of the matter effect apparently can lead to parametric resonance effects and a repopulation of ν_e from ν_x.

In all cases, the asymptotic Y_e value is lowered compared to the non-oscillation case, but it sensitively depends on the cooling phase how large this effect turns out to be. The inclusion of active-active collective oscillations and MSW conversions in addition to active-sterile mixing strongly modifies the outcome. These general trends are not severely altered

by larger values of Θ_{13}.

Accordingly, neutrino conversion to a sterile flavor as well as oscillations and collective transformations of active flavors influence the radial variation and time-dependent asymptotic value of Y_e in the neutrino-driven wind in complicated ways. The feedback of active-sterile oscillations on the refractive effect causes intriguing nonlinear modifications of the naive oscillation picture and active-active oscillations can in addition play an important role in determining the neutron-to-proton ratio of SN ejecta.

The chemical composition of the matter outflow can thus be strongly affected by neutrino oscillations. In our model of the neutrino cooling of the proto-neutron star born in an electron-capture SN, the corresponding changes do not lead to a large neutron excess. Therefore it appears unlikely that in the studied cases viable r-process conditions could be produced by flavor oscillations, although the formation of heavy elements must be expected to change.

All numerical studies of neutrino oscillations with neutrino-neutrino refraction use simplified assumptions, in our case the "single angle approximation," but even more sophisticated "multi-angle studies" assume axial symmetry around the radial direction and therefore are not fully general. Even if we suspect that our conclusions are not affected by the ν–ν interaction's angular dependence, a careful analysis on this effect remains certainly to be investigated.

More important may be the calculation of a denser grid of snapshots for more solid conclusions on the nucleosynthetic implications and as the basis for detailed studies of element formation. Moreover, because the neutrino emission properties and the neutrino-driven wind conditions depend sensitively on the mass of the proto-neutron star [51], our results for the $1.36\,M_\odot$ (baryonic mass) remnant of an electron-capture SN may be applicable only to SNe with similar compact objects. The investigation of a broader range of progenitor models, in particular also of iron-core SNe with more massive proto-neutron stars, is therefore desirable to identify possible cases where favorable conditions for the r-process may be produced by flavor oscillations involving sterile neutrinos.

If sterile neutrinos with parameters suggested by the presently discussed antineutrino reactor anomaly are verified in future experiments, their existence cannot be ignored in nucleosynthesis studies of the SN environment. Sterile neutrinos must be expected to have important consequences for the possibility of a νp-process in SN outflows and might even be relevant for the question whether SN explosions can be sources of r-process elements. The experimental neutrino mixing parameters will be a crucial input information for theoretical investigations of these problems.

References

[1] A. Aguilar *et al.* (LSND Collaboration), "Evidence for neutrino oscillations from the observation of $\bar{\nu}_e$ appearance in a $\bar{\nu}_\mu$ beam," Phys. Rev. D **64**, 112007 (2001) [hep-ex/0104049].

[2] A. Strumia, "Interpreting the LSND anomaly: sterile neutrinos or CPT-violation or...?," Phys. Lett. B **539**, 91 (2002) [hep-ph/0201134].

[3] M. C. Gonzalez-Garcia and M. Maltoni, "Phenomenology with Massive Neutrinos," Phys. Rept. **460**, 1 (2008) [arXiv:0704.1800].

[4] A. A. Aguilar-Arevalo *et al.* (MiniBooNE Collaboration), "Unexplained excess of electron-like events from a 1-GeV neutrino beam," Phys. Rev. Lett. **102**, 101802 (2009) [arXiv:0812.2243].

[5] A. A. Aguilar-Arevalo *et al.* (MiniBooNE Collaboration), "A search for electron antineutrino appearance at the $\Delta m^2 \sim 1$ eV^2 scale," Phys. Rev. Lett. **103**, 111801 (2009) [arXiv:0904.1958].

[6] G. Karagiorgi, Z. Djurcic, J. M. Conrad, M. H. Shaevitz and M. Sorel, "Viability of $\Delta m^2 \sim 1$ eV^2 sterile neutrino mixing models in light of MiniBooNE electron neutrino and antineutrino data from the Booster and NuMI beamlines," Phys. Rev. D **80**, 073001 (2009); Erratum ibid. D **81**, 039902 (2010) [arXiv:0906.1997].

[7] E. Akhmedov and T. Schwetz, "MiniBooNE and LSND data: Non-standard neutrino interactions in a (3+1) scheme versus (3+2) oscillations," JHEP **1010** (2010) 115 [arXiv:1007.4171].

[8] S. Razzaque and A. Yu. Smirnov, "Searching for sterile neutrinos in ice," JHEP **1107** (2011) 084 [arXiv:1104.1390].

[9] B. A. Reid, L. Verde, R. Jimenez and O. Mena, "Robust neutrino constraints by combining low redshift observations with the CMB," JCAP **1001** (2010) 003 [arXiv:0910.0008].

[10] M. C. Gonzalez-Garcia, M. Maltoni and J. Salvado, "Robust cosmological nounds on neutrinos and their combination with oscillation results," JHEP **1008**, 117 (2010) [arXiv:1006.3795].

[11] J. Hamann, S. Hannestad, G. G. Raffelt, I. Tamborra and Y. Y. Y. Wong, "Cosmology favoring extra radiation and sub-eV mass sterile neutrinos as an option," Phys. Rev. Lett. **105** (2010) 181301 [arXiv:1006.5276].

[12] E. Giusarma, M. Corsi, M. Archidiacono, R. de Putter, A. Melchiorri, O. Mena and S. Pandolfi, "Constraints on massive sterile neutrino species from current and future cosmological data," Phys. Rev. D **83** (2011) 115023 [arXiv:1102.4774].

[13] Z. Hou, R. Keisler, L. Knox, M. Millea and C. Reichardt, "How additional massless neutrinos affect the cosmic microwave background damping tail," arXiv:1104.2333.

[14] Y. I. Izotov and T. X. Thuan, "The primordial abundance of 4He: evidence for non-standard big bang nucleosynthesis," Astrophys. J. **710** (2010) L67 [arXiv:1001.4440].

[15] E. Aver, K. A. Olive and E. D. Skillman, "A new approach to systematic uncertainties and self-consistency in helium abundance determinations," JCAP **1005** (2010) 003 [arXiv:1001.5218].

[16] J. Hamann, S. Hannestad, G. G. Raffelt and Y. Y. Y. Wong, "Sterile neutrinos with eV masses in cosmology – how disfavoured exactly?," JCAP **1109** (2011) 034 [arXiv:1108.4136].

[17] G. Mention, M. Fechner, T. Lasserre, T. A. Mueller, D. Lhuillier, M. Cribier and A. Letourneau, "The reactor antineutrino anomaly," Phys. Rev. D **83** (2011) 073006 [arXiv:1101.2755].

[18] P. Huber, "On the determination of anti-neutrino spectra from nuclear reactors," Phys. Rev. **C84** (2011) 024617 [arXiv:1106.0687].

[19] J. Kopp, M. Maltoni and T. Schwetz, "Are there sterile neutrinos at the eV scale?," Phys. Rev. Lett. **107** (2011) 091801 [arXiv:1103.4570].

[20] S. Chakraborty, T. Fischer, A. Mirizzi, N. Saviano and R. Tomàs, "Analysis of matter suppression in collective neutrino oscillations during the supernova accretion phase," Phys. Rev. D **84**, 025002 (2011) [arXiv:1105.1130].

[21] S. Sarikas, G. G. Raffelt, L. Hüdepohl and H.-T. Janka, "Flavor stability of a realistic accretion-phase supernova neutrino flux," arXiv:1109.3601.

[22] B. Dasgupta, E. P. O'Connor and C. D. Ott, "The role of collective neutrino flavor oscillations in core-collapse supernova shock revival," arXiv:1106.1167.

[23] Y. Suwa, K. Kotake, T. Takiwaki, M. Liebendörfer and K. Sato, "Impacts of collective neutrino oscillations on core-collapse supernova explosions," Astrophys. J. **738**, 165 (2011) [arXiv:1106.5487].

[24] M. Arnould, S. Goriely and K. Takahashi, "The r-process of stellar nucleosynthesis: Astrophysics and nuclear physics achievements and mysteries," Phys. Rept. **450**, 97 (2007) [arXiv:0705.4512].

[25] J. Beun, G. C. McLaughlin, R. Surman and W. R. Hix, "Fission cycling in supernova nucleosynthesis: Active-sterile neutrino oscillations," Phys. Rev. D **73** (2006) 093007 [hep-ph/0602012].

[26] P. Keranen, J. Maalampi, M. Myyrylainen and J. Riittinen, "Sterile neutrino signals from supernovae," Phys. Rev. **D76** (2007) 125026 [arXiv:0708.3337].

[27] J. Fetter, G. C. McLaughlin, A. B. Balantekin and G. M. Fuller, "Active sterile neutrino conversion: Consequences for the r process and supernova neutrino detection," Astropart. Phys. **18** (2003) 433 [hep-ph/0205029].

[28] J. M. Fetter, "Resonant active sterile neutrino conversion and r process nucleosynthesis in neutrino heated supernova ejecta," PhD Thesis (University of Wisconsin, 2000).

[29] G. C. McLaughlin, J. M. Fetter, A. B. Balantekin and G. M. Fuller, "An Active sterile neutrino transformation solution for r process nucleosynthesis," Phys. Rev. **C59** (1999) 2873 [astro-ph/9902106].

[30] J. Hidaka and G. M. Fuller, "Sterile neutrino-enhanced supernova explosions," Phys. Rev. **D76** (2007) 083516 [arXiv:0706.3886].

[31] H. Nunokawa, J. T. Peltoniemi, A. Rossi and J. W. F. Valle, "Supernova bounds on resonant active sterile neutrino conversions," Phys. Rev. **D56** (1997) 1704 [hep-ph/9702372].

[32] H. Duan, G. M. Fuller and Y.-Z. Qian, "Collective neutrino oscillations," Ann. Rev. Nucl. Part. Sci. **60** (2010) 569 [arXiv:1001.2799].

[33] H. Duan, A. Friedland, G. C. McLaughlin and R. Surman, "The influence of collective neutrino oscillations on a supernova r-process," J. Phys. G **G38** (2011) 035201 [arXiv:1012.0532].

[34] G. Martínez-Pinedo, B. Ziebarth, T. Fischer and K. Langanke, "Effect of collective neutrino flavor oscillations on vp-process nucleosynthesis," arXiv:1105.5304.

[35] L. Hüdepohl, B. Müller, H.-T. Janka, A. Marek and G. G. Raffelt, "Neutrino signal of electron-capture supernovae from core collapse to cooling," Phys. Rev. Lett. **104** (2010) 251101 [arXiv:0912.0260].

[36] S. Wanajo, K. Nomoto, H.-T. Janka, F. S. Kitaura and B. Müller, "Nucleosynthesis in electron capture supernovae of AGB stars," Astrophys. J. **695** (2009) 208 [arXiv:0810.3999].

[37] A. J. T. Poelarends, F. Herwig, N. Langer and A. Heger, "The supernova channel of super-AGB stars," Astrophys. J. **675** (2008) 614. [arXiv:0705.4643].

[38] H. Shen, H. Toki, K. Oyamatsu and K. Sumiyoshi, "Relativistic equation of state of nuclear matter for supernova and neutron star," Nucl. Phys. A **637** (1998) 435 [nucl-th/9805035].

[39] M. T. Keil, G. G. Raffelt and H.-T. Janka, "Monte Carlo study of supernova neutrino spectra formation," Astrophys. J. **590** (2003) 971 [astro-ph/0208035].

[40] H. Duan, G. M. Fuller, J. Carlson, Y.-Z. Qian, "Simulation of coherent non-linear neutrino flavor transformation in the supernova environment. 1. Correlated neutrino trajectories," Phys. Rev. **D74** (2006) 105014 [astro-ph/0606616].

[41] G. L. Fogli, E. Lisi, A. Marrone, A. Palazzo and A. M. Rotunno, "Evidence of $\theta_{13} > 0$ from global neutrino data analysis," Phys. Rev. **D84** (2011) 053007 [arXiv:1106.6028].

[42] S. P. Mikheev and A. Yu. Smirnov, "Resonance amplification of oscillations in matter and spectroscopy of solar neutrinos," Yad. Fiz. **42**, (1985) 1441 [Sov. J. Nucl. Phys. **42** (1985) 913].

[43] G. Sigl and G. Raffelt, "General kinetic description of relativistic mixed neutrinos," Nucl. Phys. **B406** (1993) 423-451.

[44] G. C. McLaughlin, G. M. Fuller and J. R. Wilson, "The influence of nuclear composition on the electron fraction in the post-core-bounce supernova environment," Astrophys. J. **472** (1996) 440 [astro-ph/9701114].

[45] S. A. Bludman and K. A. Van Riper, "Diffusion approximation to neutrino transport in dense matter," Astrophys. J. **224** (1978) 631.

[46] B. Dasgupta, A. Dighe, G. G. Raffelt and A. Yu. Smirnov, "Multiple spectral splits of supernova neutrinos," Phys. Rev. Lett. **103** (2009) 051105 [arXiv:0904.3542].

[47] G. Fogli, E. Lisi, A. Marrone and I. Tamborra, "Supernova neutrinos and antineutrinos: Ternary luminosity diagram and spectral split patterns," JCAP **0910** (2009) 002 [arXiv:0907.5115].

[48] G. L. Fogli, E. Lisi, A. Marrone and A. Mirizzi, "Collective neutrino flavor transitions in supernovae and the role of trajectory averaging," JCAP **0712** (2007) 010 [arXiv:0707.1998].

[49] G. L. Fogli, E. Lisi, A. Marrone, A. Mirizzi and I. Tamborra, "Low-energy spectral features of supernova (anti)neutrinos in inverted hierarchy," Phys. Rev. D **78** (2008) 097301 [arXiv:0808.0807].

[50] A. Esteban-Pretel, S. Pastor, R. Tomas, G. G. Raffelt and G. Sigl, "Decoherence in supernova neutrino transformations suppressed by deleptonization," Phys. Rev. D **76** (2007) 125018 [arXiv:0706.2498].

[51] Y.-Z. Qian and S.E. Woosley, "Nucleosynthesis in neutrino-driven winds. I. The physical conditions," Astrophys. J. **471** (1996) 331.